An Extended Approach to Error Control in Experimental and Numerical Data Smoothing and Evaluation Using the Meshless FDM

Józef Krok

Section of Computer Method in Mechanics
Cracow University of Technology, Cracow, Poland
plkrok@cyf-kr.edu.pl

ABSTRACT. *This work addresses the development of an approach to approximation, smoothing and error estimation of physical/numerical data. It includes: development of postprocessing techniques for approximation of data in discrete form, development of an iterative approach to additional enhancement of data at new (required in computer procedures) locations, validation of an a posteriori technique to trace loss of accuracy in original data, and application of above mentioned procedure in wheel stress recovery calculations (approximation of the physical and numerical - FEM data). Theoretical considerations and numerical analysis are based on the Adaptive Finite element Analysis (AFEM) and the Meshless Finite Difference approximation (MFDM).*

RÉSUMÉ. *Dans ce travail, nous développons une approche d'approximation, de lissage et d'estimation d'erreur pour des données physiques et numériques. Cela concerne le développement de techniques de postraitement pour approximation des données discrètes. Nous mettons en place une approche itérative pour enrichissement des données dans des nouvelles locations nécessaires pour les procédures numériques. Nous validons une technique a posteriori pour tracer la perte de précision dans les données originales. Nous appliquons ces techniques aux calculs de reconstruction des champs de contraintes dans les roues. Cela inclut l'approximation des données physiques et numériques obtenues par éléments finis. Les considérations théoriques et l'analyse numérique sont basées sur une analyse adaptative par éléments finis (AFEM) et sur l'approximation par différences finis sur grilles irrégulières (MFDM).*

KEYWORDS: *experimental data smoothing and evaluation, error control, meshless FDM.*

MOTS-CLÉS : *lissage des données, contrôle d'erreur, différences finies sur grilles irrégulières.*

REEF – 11/2002. Meshfree Computational Mechanics, pages 913 to 945

1. Introduction

This work addresses the validation of a new approach proposed to control error in smoothing/approximation of experimental and numerical data. On the base of a'posteriori error analysis of data, we introduce an adaptive procedure of experimental data collection and evaluation is presented.

One often has to transfer discrete data known at certain points to other points, for instance one may need *e.g*. a much clearer picture or require data smoothing. Sometimes one may also need additional data. How can this be done at the minimal loss of accuracy? Is it possible to measure the degree of information loss and if so, how? Is it possible to recover, as a by-product, additional information on the data (regularity, smoothness) and locations of data points (guaranteing the highest accuracy: distributions of data points density and function gradients are similar). Answers to above-mentioned questions are crucial in proper interpretation of experimental/numerical data. May one find a positive answer to these questions?

The present research is concentrated on further development of an approximation technique of physical/numerical data, based on the MWLS (Moving Weighted Least Squares) [7, 8, 9, 11] and finite difference formulae (FDM) and formulation of a new approach to experimental data measurements planning and carrying out.

It includes:

– validation of postprocessing techniques for data approximation done in a discrete form and an iterative approach to additional enhancement of data at new (required) locations,

– formulation of a posteriori error technique to trace loss of accuracy of original data by using different "error norms", a posteriori error estimation,

– evaluation of experimental points density in experimental data taking into account equal error distribution,

– formulation of the new adaptive approach to experiment planning and carrying out, taking into account a'posteriori error estimation and distribution of experimental points with equidistributed error,

– analysis of the wheel saw cut data, especially for the wheel #2 (see R.Czarnek [3], and J.Krok, J.Orkisz, A.Skrzat [11], J.Krok [8]), as an sample application of the proposed approach

Part of the theoretical considerations is based on the Adaptive Finite Element Analysis (AFEM). AFEM gives tools to solve the problem under consideration, even though the problem does not necessarily conform to the AFEM case, because several assumptions are violated (for example one does not know the rate of convergence and degree of smoothness, *i.e*. regularity of the physical data). In this work, we develop an original idea to interpret the physical data in the same way as the numerical data coming from FEM or FDM – using an adaptive analysis.

2. Approximation and error analysis of numerical and experimental data

The theory of a'posteriori error estimation in discrete methods like in the FEM or MFDM is already well established. As a result one obtains new mesh density to solve boundary value problems with highest possible accuracy *i.e.* with equidistributed errors. Now the same idea is proposed for experimental mechanics. Theory presented here allows to evaluate results obtained in experiment and to give very precise information on location and density of gauges or on size of moire interferometry grid (output of any experimental method may be evaluated). If it is not possible to improve measurement quality, one gets precise information on data measured with insufficient precision. Reliability indices defined in present work permit to take into account measurements differing in quality.

A'posteriori error estimation in FEM, which may be (however indirectly) used to introduce proposed idea, is presented here to explain our intent.

2.1. *Zienkiewicz-Zhu a posteriori error estimator*

First, for the sake of clarity of proposed experimental data approximation, the *a posteriori* error estimator used in FEM and MFDM, based on the postprocessing approach will be presented. For estimators based on the stress (or flux) recovery technique (Zienkiewicz, Zhu [14-17]) one has

$$\|e\| = [\int_{\Omega} (\sigma - \sigma^h)^T D^{-1} (\sigma - \sigma^h) d\Omega]^{\frac{1}{2}} \tag{2.1}$$

where σ^h are stresses obtained by the FEM.

The exact stresses σ are approximated by new stresses obtained using the stress recovery procedure (the Meshless Finite Difference method is used here [9,15])

$$\sigma^* = N\overline{\sigma}^* \tag{2.2}$$

where $\overline{\sigma}^*$ are nodal values obtained by the MFDM recovery procedure, and N is a shape functions matrix.

The exact solution for the strain energy is estimated as

$$\|U\| = [\int_{\Omega} (\sigma^h)^T D^{-1} (\sigma^h) d\Omega]^{\frac{1}{2}} + \|e\|^2 \tag{2.3}$$

where an error of the energy norm is expressed as

$$\|e\| = [\int_{\Omega} (\sigma^* - \sigma^h)^T D^{-1} (\sigma^* - \sigma^h) d\Omega]^{\frac{1}{2}} \tag{2.4}$$

Both $\|e\|$ and $\|U\|$ norms may be evaluated as a sum of their respective element contributions so that (n denotes the total number of elements in the mesh)

$$\|e\|^2 = \sum_{i=1}^{n} \|e\|_i^2 \,,\ \|U\|^2 = \sum_{i=1}^{n} \|U\|_i^2 \tag{2.5}$$

REMARK. — An *a posteriori* error procedure can be split into two main stages:

– stage 1: calculation of stresses (or other primary values) at Gaussian points - the primary set of points,

– stage 2: approximation of the Gaussian-located stresses at nodal positions (secondary set of points), retrieval of the nodal values to Gauss points using (for example) standard shape functions or other kind of approximation.

Having two sets of values of different accuracy at the same points, one may calculate local $\|e\|_i$, $\|U\|_i$ and global $\|e\|$, $\|U\|$ norms.

2.2. *Meshless error estimator*

New idea of a'posteriori error estimation of randomly distributed experimental data or numerical data coming from FEM or MFDM analysis is presented here.

Let us define the following problem:

– data, (not necessary stresses like in eq. (2.4)) coming from experiment, located at certain points - set #1 (see experimental points – set of primary points – figure 2.1) is given,

– the fictitious sets of points used later in calculation - set #2 (see fictitious points – set of secondary points - figure.2.1) is given.

The problem lies in data translation (approximation) from #1 points set to #2 points set. The problem is exactly the same as in error estimator (2.4), but now one has two different sets of points with, in fact, arbitrary (not elemental) locations and one has no information on regularity, smoothness and reliability of the data.

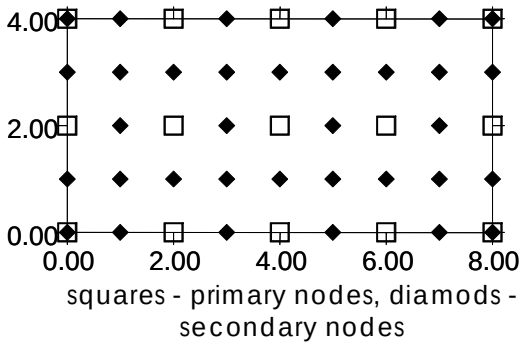

Figure 2.1. *Primary and secondary mesh for approximation of physical or numerical data*

Differences between two surfaces defined by data #1 and #2 may be measured by the norm

$$\|e\| = [\int_{\Omega} (u^* - u^h)^T (u^* - u^h) + (\nabla u^* - \nabla u^h)^T (\nabla u^* - \nabla u^h) + (\kappa u^* - \kappa u^h)^T (\kappa u^* - \kappa u^h) d\Omega]^{\frac{1}{2}} \quad (2.6)$$

where u^h is the vector of experimental data (in experimental points) and u^* is the vector of fictitious sought data. Sometimes weighting factors may be used to equilibrate dimensions of terms. In the above formula one can omit (sometimes not) the gradients and curvature terms (κ - see generalized curvature – Karmowski and Orkisz [5, 6]). One can also use discrete form of this formula, summing up differences between values at experimental points.

To solve this problem, data from experimental points is approximated to fictitious ones (using FDM approximation - see next part of this work) and later on, taking values at fictitious points as original data, approximated back from fictitious points to experimental ones. In this two-stage approximation part of data is lost, but if differences between original data in the experimental points and fictitious data in the same points are small enough, one may expect that the approximation in first step does not introduce too large error. As will be seen from numerical analysis this assumption is true.

Additionally, in the zones where the gradients of approximated function are larger, the error magnitude is considerably higher as compared to the zones with smaller data gradients. Moreover, if irregularity in data is large the error increases. Those facts may be used, as by-product important information, to evaluate experimental data. Having vector of differences between experimental and fictitious values at experimental points one can "smear" the error, approximating vector of differences from experimental to fictitious points. Adding correction to initial

fictitious values one can obtain new enhanced fictitious values. This process can be repeated (iteration process gives possibility to avoid fluctuation, especially when data is very smooth, like MFDM solution). In this way, the usual approach elaborated mainly in adaptive Finite Element Method is unified, extended and generalized.

The total norm of the measured values may be expressed as (the discrete form of the below norms may be used):

$$\|U\|^2 = [\int_\Omega (u^h)^T u^h + (\nabla u^h)^T \nabla u^h + (\kappa u^h)^T \kappa u^h d\Omega] + \|e\|^2 \tag{2.7}$$

The key question is, whether one can evaluate experimental data using norms (2.6) and (2.7)? The answer is yes, if data are regular enough.

As one can see from equation (2.7), not only values of a function measured, but gradients of the function and curvatures are taken into account as well. Additionally, one can considerably improve coarse FEM solution, using MFDM approximation to find any required derivatives at any point of domain, with error control as a by-product.

3. Meshless finite difference approximation

The approximation $u^h(\mathbf{x})$ of function $u(\mathbf{x})$ is posed as polynomial of order m with non-constant coefficients $a_0(\mathbf{x}), a_1(\mathbf{x}),..., a_m(\mathbf{x})$. The order of polynomial is defined as the order of the basis. For a linear basis in two dimensions $u^h(\mathbf{x})$ can be written as

$$u^h(\mathbf{x}) = a_0 + a_1 x + a_2 y\,, \tag{3.1}$$

where unknown parameters $a_j(\mathbf{x})$ vary with **x.** The local approximation (for $\bar{\mathbf{x}} = \mathbf{x}$) is given by [1, 9, 10, 15]

$$u^h(\mathbf{x}, \bar{\mathbf{x}}) = \sum_{j=0}^{m} p\ (\mathbf{x}) a_j(\bar{\mathbf{x}}) = \mathbf{p}^T(\mathbf{x})\mathbf{a}(\mathbf{x}) \tag{3.2}$$

where $\mathbf{p}(\mathbf{x})$ is a complete polynomial of order *m*

$$\mathbf{p}^T(\mathbf{x}) = [1, x, y, x^2, xy, y^2,...,] \tag{3.3}$$

and $\mathbf{a}(\mathbf{x})$ is given by

$$\mathbf{a}^T(\mathbf{x}) = [a_0(\mathbf{x}), a_1(\mathbf{x}),..., a_m(\mathbf{x})]. \tag{3.4}$$

The unknown parameters $a_j(\mathbf{x})$ at any given point are determined by minimizing the difference between the local approximation at that point and the nodal parameters u_I *i.e.* weighted, discrete L_2 norm

$$J(\mathbf{a}) = \sum_{I=1}^{n} w(\mathbf{x}-\mathbf{x}_I)[u^h(\mathbf{x}_I,\mathbf{x}) - u_I]^2 = \sum_{I=1}^{n} w(\mathbf{x}-\mathbf{x}_I)[p^T(\mathbf{x}_I)a(\mathbf{x}) - u_I]^2, \tag{3.5}$$

where $w(\mathbf{x}-\mathbf{x}_I)$ is a shift of a given weighting function $w(\mathbf{x})$, and *n* is the number of nodes in the neighborhood of **x** for which the weighting function $w(\mathbf{x}-\mathbf{x}_I) \neq 0$.

The minimum of *J* in (3.5) with respect to $\mathbf{a}(\mathbf{x})$ leads to the following set of linear equations

$$\mathbf{A}(\mathbf{x})\mathbf{a}(\mathbf{x}) = \mathbf{B}(\mathbf{x})\mathbf{u}. \tag{3.6}$$

After solving the set of equations (3.6), one obtains

$$\mathbf{a}(\mathbf{x}) = \mathbf{A}^{-1}(\mathbf{x})\mathbf{B}(\mathbf{x})\mathbf{u} = \sum_{I=1}^{n} \mathbf{A}^{-1}(\mathbf{x})\mathbf{B}_I(\mathbf{x})u_I = \mathbf{Q}(\mathbf{x})\mathbf{u}, \tag{3.7}$$

where

$$\mathbf{A}(\mathbf{x}) = \sum_{I=1}^{n} w(\mathbf{x}-\mathbf{x}_I)\mathbf{p}(\mathbf{x}_I)\mathbf{p}^T(\mathbf{x}_I) \quad , \tag{3.8}$$

$$\mathbf{B}(\mathbf{x}) = [w(\mathbf{x}-\mathbf{x}_1)\mathbf{p}(\mathbf{x}_1),\ w(\mathbf{x}-\mathbf{x}_2)\mathbf{p}(\mathbf{x}_2),..., w(\mathbf{x}-\mathbf{x}_n)\mathbf{p}(\mathbf{x}_n)] \tag{3.9}$$

Substituting (3.7) into (3.2), the MWLS approximants can be defined as

$$u^h = \mathbf{p}^T(\mathbf{x})\mathbf{A}^{-1}(\mathbf{x})\mathbf{B}(\mathbf{x})\mathbf{u} = \sum_{I=1}^{n}\sum_{j-0}^{m} p_j(\mathbf{x})[\mathbf{A}^{-1}(\mathbf{x})\mathbf{B}(\mathbf{x})]_{jI}u_I = \sum_{I=1}^{n} \tilde{N}_I(\mathbf{x})u_I = \tilde{\mathbf{N}}\mathbf{u}, \tag{3.10}$$

where

$$\tilde{N}_I(\mathbf{x}) = \sum_{j=0}^{m} p_j(\mathbf{x})[\mathbf{A}^{-1}(\mathbf{x})\mathbf{B}(\mathbf{x})]_{jI} = \mathbf{p}^T\mathbf{A}^{-1}\mathbf{B}_I = \sum_{j=1}^{m} p_j Q_{jI} \tag{3.11}$$

are the shape functions in MWLS approximation (note that $\sum_{I}^{n} \tilde{N}_I = 1$).

To determine the derivatives of the approximating function $u^h(\mathbf{x})$, one has to obtain the shape functions' derivatives. The spatial derivatives of the shape functions are determined by

$$\tilde{N}_{I,x} = [\mathbf{p}^T \mathbf{A}^{-1} \mathbf{B}_I]_{,x} = \mathbf{p}^T{}_{,x} \mathbf{A}^{-1} \mathbf{B}_I + \mathbf{p}^T \mathbf{A}^{-1}{}_{,x} \mathbf{B}_I + \mathbf{p}^T \mathbf{A}^{-1} \mathbf{B}_{I,x}, \quad (3.12)$$

where

$$\mathbf{B}_I(\mathbf{x}) = \frac{\partial w(\mathbf{x} - \mathbf{x}_I)}{\partial x} \mathbf{p}(\mathbf{x}_I). \quad (3.13)$$

Matrix $\mathbf{A}_{,x}^{-1}$ is computed by

$$\mathbf{A}_{,x}^{-1} = -\mathbf{A}^{-1} \mathbf{A}_{,x} \mathbf{A}^{-1} \quad (3.14)$$

where

$$A_{,x} = \sum_{I=1}^{n} \frac{\partial w(\mathbf{x} - \mathbf{x}_I)}{\partial x} \mathbf{p}(\mathbf{x}_I) \mathbf{p}^T(\mathbf{x}_I). \quad (3.15)$$

To compute the shape functions and their derivatives, the **A** matrix has to be inverted. This process is more computationally efficient if LU decomposition of the matrix **A** is performed. The shape functions in (3.11) can be written as

$$\tilde{N}_I = \sum_{j=0}^{m} p_j(\mathbf{x}) \mathbf{A}^{-1}(\mathbf{x}) \mathbf{B}_{jI}(\mathbf{x}) = \mathbf{p}^T \mathbf{A}^{-1} \mathbf{B}_I = \mathbf{g}^T \mathbf{B}_I, \quad (3.16)$$

where the following relationship was used [1]

$$\mathbf{A}(\mathbf{x}) \mathbf{g}(\mathbf{x}) = \mathbf{p}(\mathbf{x}). \quad (3.17)$$

The vector $\mathbf{g}(\mathbf{x})$ can be determined the same way as the **a** vector. The derivatives of vector $\mathbf{g}(\mathbf{x})$ can be computed similarly, this leads to a computationally efficient procedure to determine derivatives of u^h. Taking spatial derivatives of (3.17) and rearranging these, one has

$$\mathbf{A}(\mathbf{x})\mathbf{g}(\mathbf{x})_{,x} = \mathbf{p}(\mathbf{x})_{,x} - \mathbf{A}_{,x}\mathbf{g}. \tag{3.18}$$

Thus, the derivative of $\mathbf{g}(\mathbf{x})$ can be calculated using the same **LU** decomposition obtained from (3.17). Spatial derivatives of shape function may be obtained as [1]

$$\tilde{N}_I(\mathbf{x})_{,x} = \mathbf{g}(\mathbf{x})_{,x}\mathbf{B}_I + \mathbf{g}(\mathbf{x})\mathbf{B}_{I,x}. \tag{3.19}$$

By consecutive derivation of equation (3.18) one obtains the set of following equations for vector $\mathbf{g}$ and its derivatives (once more note that the **LU** decomposition of **A** matrix is performed only once):

$$\begin{aligned}
&\mathbf{A}(\mathbf{x})\mathbf{g}(\mathbf{x}) = \mathbf{p}(\mathbf{x}),\\
&\mathbf{A}(\mathbf{x})\mathbf{g}(\mathbf{x})_{,x} = \mathbf{p}(\mathbf{x})_{,x} - \mathbf{A}_{,x}\mathbf{g},\\
&\mathbf{A}(\mathbf{x})\mathbf{g}(\mathbf{x})_{,y} = \mathbf{p}(\mathbf{x})_{,y} - \mathbf{A}_{,y}\mathbf{g},\\
&\mathbf{A}(\mathbf{x})\mathbf{g}(\mathbf{x})_{,xx} = \mathbf{p}(\mathbf{x})_{,xx} - \mathbf{A}_{,xx}\mathbf{g} - 2\mathbf{A}_{,x}\mathbf{g}_{,x},\\
&\mathbf{A}(\mathbf{x})\mathbf{g}(\mathbf{x})_{,xy} = \mathbf{p}(\mathbf{x})_{,xy} - \mathbf{A}_{,xy}\mathbf{g} - \mathbf{A}_{,x}\mathbf{g}_{,y} - \mathbf{A}_{,y}\mathbf{g}_{,x},\\
&\mathbf{A}(\mathbf{x})\mathbf{g}(\mathbf{x})_{,yy} = \mathbf{p}(\mathbf{x})_{,yy} - \mathbf{A}_{,yy}\mathbf{g} - 2\mathbf{A}_{,y}\mathbf{g}_{,y}.
\end{aligned} \tag{3.20}$$

This leads to a simple relationship for the derivatives of the shape functions up to the second order

$$\begin{aligned}
&\tilde{N}_I = \mathbf{g}(\mathbf{x})\mathbf{B}_I,\\
&\tilde{N}_{I,x} = \mathbf{g}(\mathbf{x})_{,x}\mathbf{B}_I + \mathbf{g}(\mathbf{x})\mathbf{B}_{I,x},\\
&\tilde{N}_{I,y} = \mathbf{g}(\mathbf{x})_{,y}\mathbf{B}_I + \mathbf{g}(\mathbf{x})\mathbf{B}_{I,y},\\
&\tilde{N}_{I,xx} = \mathbf{g}(\mathbf{x})_{,xx}\mathbf{B}_I + 2\mathbf{g}(\mathbf{x})_{,x}\mathbf{B}_{I,x} + \mathbf{g}(\mathbf{x})\mathbf{B}_{I,xx},\\
&\tilde{N}_{I,xy} = \mathbf{g}(\mathbf{x})_{,xy}\mathbf{B}_I + \mathbf{g}(\mathbf{x})_{,x}\mathbf{B}_{I,y} + \mathbf{g}(\mathbf{x})_{,y}\mathbf{B}_{I,x} + \mathbf{g}(\mathbf{x})\mathbf{B}_{I,xy},\\
&\tilde{N}_{I,yy} = \mathbf{g}(\mathbf{x})_{,yy}\mathbf{B}_I + 2\mathbf{g}(\mathbf{x})_{,y}\mathbf{B}_{I,y} + \mathbf{g}(\mathbf{x})\mathbf{B}_{I,yy}.
\end{aligned} \tag{3.21}$$

In practical calculations, the local coordinate system $\mathbf{h} = \mathbf{h}(h,k)$ is used

$$\mathbf{h} = \mathbf{h}(h,k) = \mathbf{x} - \mathbf{x}_0,\ \mathbf{x}_0 = (x_0, y_0), \tag{3.22}$$

where $\mathbf{x}_0 = \mathbf{x}_0(x_0, y_0)$ is the point in which approximation is sought. The base vector is taken as

$$p^T = [1, h, k, \frac{1}{2}h^2, hk, \frac{1}{2}k^2, ...,], \tag{3.23}$$

so coefficients $a_0, a_1, ..., a_m$ may be immediately interpreted as derivatives at point $\mathbf{x}_o$ (usualy called local derivatives)

$$a_0 = u_0,\ a_1 = \frac{\partial u_0}{\partial x},\ a_2 = \frac{\partial u_0}{\partial y}, ..., \tag{3.24}$$

and the matrix $\mathbf{Q}$ (see 3.7) now is a generalized FD matrix. Combination of rows of this matrix and a vector of nodal values yields immediately values of function and it's derivatives at point $\mathbf{x}_0$ (but these derivatives may be not continuos from point to point).

Consistent Meshless Finite Difference matrix $\tilde{\mathbf{Q}}$ and the approximation rule now have the form

$$\mathbf{D}u = \begin{Bmatrix} u \\ u_x \\ u_y \\ u_{xx} \\ u_{xy} \\ u_{yy} \end{Bmatrix} = \begin{bmatrix} \tilde{N}_1 & \tilde{N}_2 & \cdots & \tilde{N}_n \\ \frac{\partial \tilde{N}_1}{\partial x} & \frac{\partial \tilde{N}_2}{\partial x} & \cdots & \frac{\partial \tilde{N}_n}{\partial x} \\ \cdots & \cdots & \cdots & \cdots \\ \frac{\partial^2 \tilde{N}_1}{\partial y^2} & \frac{\partial^2 \tilde{N}_2}{\partial y^2} & \cdots & \frac{\partial^2 \tilde{N}_n}{\partial y^2} \end{bmatrix} \begin{Bmatrix} u_1 \\ u_2 \\ \cdots \\ u_n \end{Bmatrix} = \tilde{\mathbf{Q}}\mathbf{u} \tag{3.25}$$

The explicit form of the matrix $\tilde{\mathbf{Q}}$ has the following form (note that matrix $\mathbf{Q}_I$ contains columns of the approximation matrix **Q** of zero-th order)

$$\tilde{\mathbf{Q}} = \begin{bmatrix} \mathbf{p}^T\mathbf{Q}_1 & \cdots & \mathbf{p}^T\mathbf{Q}_n \\ \mathbf{p}_{,x}^T\mathbf{Q}_1 + \mathbf{p}^T\mathbf{Q}_{1,x} & \cdots & \mathbf{p}_{,x}^T\mathbf{Q}_n + \mathbf{p}^T\mathbf{Q}_{n,x} \\ \mathbf{p}_{,y}^T\mathbf{Q}_1 + \mathbf{p}^T\mathbf{Q}_{1,y} & \cdots & \mathbf{p}_{,y}^T\mathbf{Q}_n + \mathbf{p}^T\mathbf{Q}_{n,y} \\ \mathbf{p}_{,xx}^T\mathbf{Q}_1 + 2\mathbf{p}_{,x}^T\mathbf{Q}_{1,x} + \mathbf{p}^T\mathbf{Q}_{1,xx} & \cdots & \mathbf{p}_{,xx}^T\mathbf{Q}_n + 2\mathbf{p}_{,x}^T\mathbf{Q}_{n,x} + \mathbf{p}^T\mathbf{Q}_{n,xx} \\ \mathbf{p}_{,xy}^T\mathbf{Q}_1 + \mathbf{p}_{,x}^T\mathbf{Q}_{1,y} + \mathbf{p}_{,y}^T\mathbf{Q}_{1,x} + \mathbf{p}^T\mathbf{Q}_{1,xy} & \cdots & \mathbf{p}_{,xy}^T\mathbf{Q}_n + \mathbf{p}_{,x}^T\mathbf{Q}_{n,y} + \mathbf{p}_{,y}^T\mathbf{Q}_{n,x} + \mathbf{p}^T\mathbf{Q}_{n,xy} \\ \mathbf{p}_{,yy}^T\mathbf{Q}_1 + 2\mathbf{p}_{,y}^T\mathbf{Q}_{1,y} + \mathbf{p}^T\mathbf{Q}_{1,yy} & \cdots & \mathbf{p}_{,yy}^T\mathbf{Q}_n + 2\mathbf{p}_{,y}^T\mathbf{Q}_{n,y} + \mathbf{p}^T\mathbf{Q}_{n,yy} \end{bmatrix} \tag{3.26}$$

Taking into accout that approximation is sought in the origin of local coordinate system one has $p^T(\mathbf{0}) = [1,0,0,0,0,0,...,]$, and thus (note: Q_{1i} is the first element in each i-th column $\mathbf{Q}_i$ of FD matrix)

$$\tilde{N}_i = \mathbf{p}^T \mathbf{Q}_i = Q_{1i}, \tag{3.27}$$

As one may see from equation (3.27) *global* shape functions are equal to *first row elements of FD matrix.*

This means that global approximation is exactly the same as local one in origin of local coordinate system. The meshless shape functions and the diffuse derivatives result naturally from the moving least squares formulation introduced in the scope of computational mechanics [Liszka Orkisz, 1980, Liszka 1984]. Further bibliography and historical details may be found in the reference book [Zienkiewicz 2000].

Relation (3.25) is valid for a very wide class of messhless approaches and yields continuous derivatives up to the second order very easily. Having two different approximation matrices: $\mathbf{Q}$ - obtained from the MWLS approximation (see equation (3.7)) and $\tilde{\mathbf{Q}}$ - (3.25) – obtained by means of the direct differentiation of $u^h(\mathbf{x})$, one has another, very useful, capability to measure error as a violation of continuity in approximation of the first and second derivatives. This way one may have at the same time two different approximation matrices.

Continuity feature of derivatives is not always beneficial, especially when approximation of data given in a set of arbitrarily spaced points is needed. Besides, there are problems with proper definition of a weighting function on arbitrarily spaced grid of points, because results of approximation, especially derivative values strongly depend on type of weighting functions used (dimensions of weight support). If support of the weighting function is not properly correlated with grid density and its form is not appropriate for the purpose required, results may be considerably worse than in the case of direct MWLS MFDM approximation. If support of approximant is too large, approximation is too smooth and thus local peak values of approximated function are anihilated.

Weighting function used here is [5, 6]

$$w(\rho) = \left(\rho^2 + \frac{g^4}{g^2 + \rho^2} \right)^{-(p+1)}, \tag{3.28}$$

where ρ is the distance between central point and the node, p denotes polynomial order and g is an optimality parameter making singular weighting

function (interpolation) or non-singular weights (approximation) available. If the optimality parameter g tends to a small value, the weighting function enforces interpolation. If optimality parameter tends to large number, approximation takes place, but data smoothing may be over emphasized.

It is worth to mention that the continuity problem arises in the MWLS approximation. Continuity requires that either all nodes in considered domain are taken into account each time or weighting functions defined on an appropriate finite supports are used providing zero end conditions. If such support is not properly corelated with the mesh density, approximation results may be of considerably lower quality than they could be. On the other hand continuity feature of MWLS approximation and its derivatives may be not neede in practice (see [12, 13]).

Test problem [12]

Though the matter requires a deeper and systematic study (see [12]) a valuable insight into the MWLS approximation quality was gained by analysis of a simple test.

Considered was a set of data presenting the values of function $u = \sqrt{25 - x^2}$ defined at nodes of an evenly spaced mesh: 0, 0.5, 1.0, 1.5, 2.0, 2.5, 3.0 having the increment 0.5.

The local (3.24) and global (3.10) MWLS approximation was performed for the function itself and for its first local (3.24) and global (3.12) derivatives. Results of error analysis obtained in the interval [0.5, 3.0] for various weighting functions are presented and compared in Figure. 3.1 a and b. The following may be noticed then:

– results of the local (3rd order) and global (consistent) approximation are, of course, the same for the function itself when using the same weighting functions.

– neither method did show clear advantages with respect to result quality when comparing the first derivative found by means of either the local (3.24) or the global (consistent) (3.12) differentiation approach. For local derivatives superconvergence property at internal nodes is noted (error of the local derivatives is considerably lower than error of the consistent derivatives). Superconvergence property of local derivatives for lower approximation order is much stronger, than for higher order (not presented here). On the other hand approximation error of the consistent derivatives is more uniform. Maximal error is lower than approximation error of the local derivatives. It is interesting to see, that the gap between local and global derivatives is proportional to the approximation error. This fact explains why error estimator proposed by Gavette, Cuesta and Ruiz works very well [18]. Probably, for the first time, it is possible to define very convenient error estimator in meshless methods, based on postprocessing, but for the two different types of derivatives.

– squared weighting functions proved clear advantage (minimal errors) over non-squared ones,

– the smallest errors in the function approximation were observed when the singular weighting factor (3.26) was used , while squared non-singular 3rd order spline weight [1], was found the best for derivative evaluation.

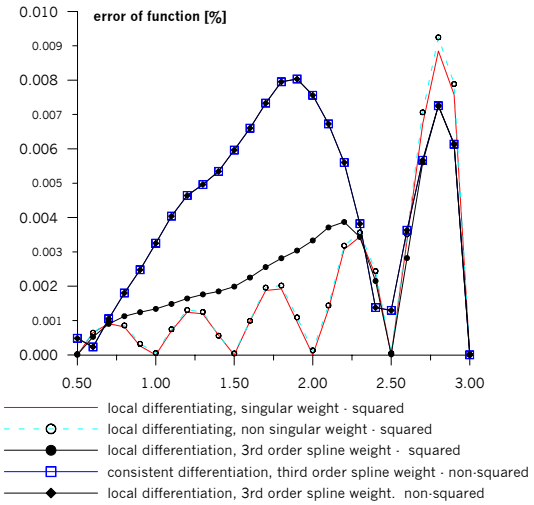

Figure 3.1a. *Weight function influence on results of approximation - function error data sought at points: min=0.5, max=3.0, increment* $\Delta x = 0.1$

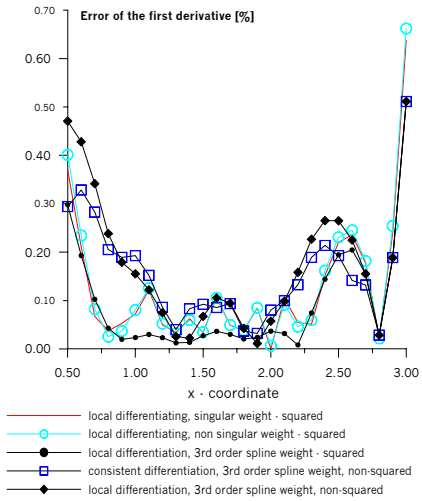

Figure 3.1b. *Weight function influence on results of approximation-derivative error*

From above test it is evident, that there are two problems: 1^0 discrete data approximation problem, 2^0 boundary-value solution problem. It is not justified to extend conclusion from data approximation to solution of boundary value problem. Even if approximation works well in data approximation, one may not obtain good results when boundary-value problem solution is needed. On the other hand bad results of data approximation not neccessarily mean that approximation will give bad results during solution of boundary-value problem.

4. Definition of the points density function in experimental and numerical discrete data

4.1. *Acceptable solution and mesh (grid) refinements function*

In an adaptive solution approach, the *a posteriori* errors are used for appropriate mesh modifications by means of the so-called error indicators and mesh refinement parameters. An approach to mesh modification applied to the adaptive FEM (or validation of a density of experimental points) is discussed below. This problem is very important because one has to have the capability to take into account, in numerical as well as in physical experiments, relation between gradients of the measured function and density (location) of the points at which information is available.

Solution is 'correct' if the two following conditions are satisfied:

(i) The global error in energy norm is less than a specified percentage value of the total strain energy

$$\|e\| = \eta \|U\| \tag{4.1}$$

where η is the 'USER' specified value of a permissible relative global error.

(ii) Distribution of elements in a new mesh satisfies a local mesh optimality criterion

$$\|e\|_i = \|e\|_{all(i)} \tag{4.2}$$

where $\|e\|_i$ is the actual error norm in i-th element and $\|e\|_{all(i)}$ is the 'required ' error norm in the element.

The global and local error parameters may be defined from equations (4.1) and (4.2) as

$$\xi_g = \frac{\|e\|}{\eta\|U\|}, \quad \bar{\xi}_i = \frac{\|e\|_i}{\|e\|_{all(i)}}. \tag{4.3}$$

The mesh refinement parameter for the i-th element is introduced as a combination of the global and local parameters [2]

$$\xi_i = \bar{\xi}_i \xi_g = \frac{\|e\|\|e\|_i}{\eta\|U\|\|e\|_{all(i)}}. \tag{4.4}$$

One of the most important questions is: how one can define the required error norm for each element. The following definitions are considered here:

(i) the global error, equally distributed all over elements in the mesh (Zienkiewicz -Zhu [15])

$$\|e\|_{all(i)} = \frac{\|e\|}{\sqrt{n}}, \tag{4.5}$$

where n is the total number of elements in a mesh.

(ii) mesh is optimal if squared error per unit element volume is the same over the whole mesh *i.e.* (Bugeda, Onate [2]), taking also into account equation (4.2) one has

$$\frac{\|e\|_i}{(\Omega_i)^{\frac{1}{2}}} = \frac{\|e\|}{(\Omega)^{\frac{1}{2}}}, \text{ and } \|e\|_i = \|e\|_{all(i)} = \|e\|\left(\frac{\Omega_i}{\Omega}\right)^{\frac{1}{2}} \tag{4.6}$$

Using eqs (4.5) and (4.6) one may obtain the following *element refinement parameters*

$$\xi_i = \frac{\|e\|_i}{\eta\|U\|(n)^{-\frac{1}{2}}}, \; \xi_i = \frac{\|e\|_i}{\eta\|U\|}\left(\frac{\Omega}{\Omega_i}\right)^{\frac{1}{2}} \tag{4.7}$$

for equal error distribution [15] and for the equal specific error distribution [2]. However, one should notice that the element and global error norms have different orders of convergence

$$\|e\|_i \approx O(h_i^m)\Omega^{\frac{1}{2}} \approx O(h_i^{m+\frac{d}{2}}),\ \|e\| \approx O(h^m) \tag{4.8}$$

where h_i and h are the i-th element size and average size of all the elements in the mesh, m is the element order and d is the problem dimension. Dividing the element error by its area one obtains

$$\frac{\|e\|_i}{(\Omega_i)^{\frac{1}{2}}} \approx O(h_i^m) \tag{4.9}$$

and new element size parameter may be defined as (this is valid only for FEM)

$$\xi_{new} = (\overline{\xi_i \xi_g})^{\frac{1}{m}} = (\xi_i)^{\frac{1}{m}}. \tag{4.10}$$

Refinement of the mesh may be done in two completely different ways: breaking elements (so called constrained approximation - see Oden, Demkowicz *et al*. [4]), or remeshing (Zhu, Zienkiewicz [15]). For the purpose of this research, th remeshing technique is preferred, as it is compatible with both FEM and MFDM discretizations.

4.2. *Error and grid density evaluation in saw cut experiment*

Crack nucleation propagation and failure of railroad car wheels is greatly influenced by residual stresses existing in those wheels, as a result of manufacturing and service conditions. The knowledge of residual stress distribution in wheels is thus required. Experimental data used for residual stress reconstruction is collected during radial saw cutting of a wheel in laboratory conditions in order to relieve residual stresses and strains, see Figure. 4.1. In order to obtain reasonable residual stress estimation, the additional approximation process is applied, which simultaneously uses error estimation procedures for considered problem.

Wheel saw cut experimental data may be evaluated using equations (4.1) and (4.2). Of course, density of experimental points depends on local (4.2) condition i.e. error at experimental points must be bound by certain admissible value. *The global and local error refinement parameters* may be defined from equations (4.1) and (4.2) as in FEM analysis. Combining both global (4.1) and local (4.2) criteria one obtains the same formula *for the mesh refinement parameter* at the i-th experimental point like in the FEM. What does mesh refinement parameter in experiment mean? It means that an experimental value at certain points changes too rapidly when compared to the mean value and local density of experimental points. In other

words, density of experimental points must be increased in certain part of the region, it is simply to low to properly describe the gradients of the measured function. New, required density is computed by formula $(4.7)_1$ - discrete form or $(4.7)_2$ - continuos form. One can take into account a weighting factor like an area assigned to experimental point (see eq. (4.7)). This is a proper definition of the admissible error at a point. Equations (4.8), (4.9) and (4.10) are not valid here because one does not have any information on the convergence of experimental results with respect to the density of experimental points. This very important problem is still open.

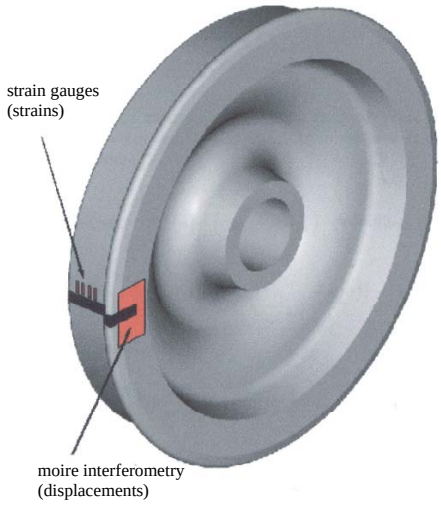

Figure 4.1. *Measurements taken at saw cut [19]*

5. Approximation of the physical data and preliminary *a posteriori* error analysis by MFDM formulas

An error analysis described above has been applied to a problem of wheel saw cut data approximation and to calculate influence matrix coefficients (see [11]). The Meshless Finite Difference Approximation [1, 8, 9, 11] has been applied. In the presented examples fictitious (discrete!) mesh generated previously: Figure. 5.1 (flange side of the wheel) has been used and the error has been determined at the experimental points.

In numerical calculations the physical data coming form the wheel #2 cutting process have been considered. 20 different sets of data: horizontal (circumferential) and vertical (radial) displacements coming from five cuts (see R.Czarnek [3] and J.Krok [8]) of the wheel have been used in calculations.

Three different effects concerning experimental data are investigated:

1. An approximation error of the measured values from experimental grid to one used in numerical analysis.

2. Evaluation of the measured values taking into account five different 'error' norms.

3. Estimation of the new experimental points' grid density with equal distribution of an approximation error kept in mind.

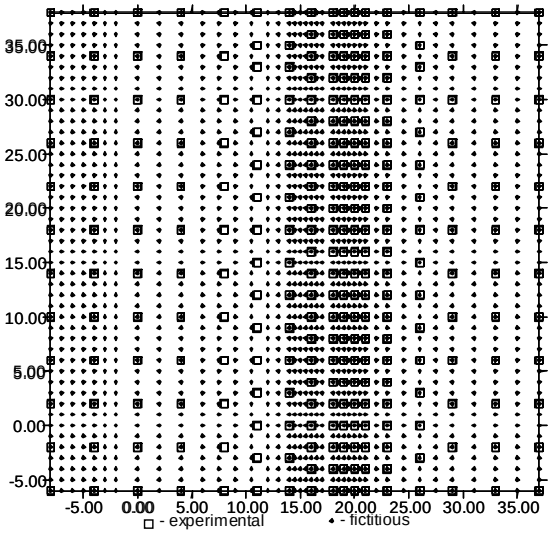

Figure 5.1. *Flange side of the wheel, Experimental and fictitious grids*

In both analyses, local as well as global error norms were considered.

An approximation of experimental data with different order and different number of nodes in stars is presented in Figure. 5.2-5.25. Notation used: n_taylor - number of coefficients in Taylor series expansion, nodes - number of nodes in star, optim_par=optimality parameter g - mean distance between current node and central point of a star.

Results obtained are plotted in Figures. 5.2 – 5.27. These pictures are divided into 3 different groups, namely:

Set #1 (Figures 5.2-5.19) - detailed analysis of data approximation performed for each of cuts: #1, #3, #5 of the wheel #2 for flange side (horizontal displacements) of the wheel with optimal approximation parameters taken into account. Approximation parameters taken into account are: n_taylor=8, nodes=36, optim_par=2.

Detailed description of the pictures is as follows:

Cut #1: Figure. 5.2, Flange side, cut #1, horizontal displacements, original data,

Figure. 5.3, Flange side, cut #1, horizontal displacements, approximated data after 7 iterations,

Figure. 5.4, Flange side, cut #1, horizontal displacements, recovered data, no iterations,

Figure. 5.5, Flange side, cut #1, error of the horizontal displacements, no iterations,

Figure. 5.6, Flange side, cut #1, horizontal displacements, recovered data after 7 iterations,

Figure. 5.7, Flange side, cut #1, error of the horizontal displacements, after 7 iterations,

Cut #3: flange side, horizontal displacements: Figures 5.8-5.13,

Cut #5: flange side, horizontal displacements: Figures 5.14-5.19,

As one can see, because the smoothness parameter has the optimum value, approximated data is smooth enough and the errors are very small. Iterations between experimental data and fictitious data considerably decrease the errors (magnitude of the error decreases approximately 10 times). In this way one may absolutely ensure that data at experimental points and data at fictitious points are very close to each other. Thus, one may use data at fictitious points for further analysis, and this process is under error control.

Set #2, cut#3 (Figures 5.20 – 5.22) - summarizing pictures concerning full evaluation of the approximation process and simultaneously experimental data, flange side - horizontal displacements: local error and grid density distribution for different 'error' norms. Detailed description of the pictures is as follows:

Flange side, horizontal displacements

Cut #3, flange side, Figure. 5.20, Error distribution and grid density distribution:

(1) horizontal displacements, (2) error norm #1 – Sobolev norm of zero order,

(3) grid density - norm #1,

(4) error norm #2 – Sobolev seminorm of first order, (5) grid density - norm #2,

(6) error norm #3 – Sobolev norm of first order, (7) grid density - norm #3,

(8) displacement curvature, (9) error norm #4 – Sobolev seminorm of second order,(10) grid density - norm #4,

(11) error norm #5 – Sobolev norm of second order, (12) grid density - norm #5.

Approximated experimental data may be filtered, using a certain treshold value. In Figures 5.21 and 5.22 area where required grid density is greater than 1.0% is shown for cut #3:

Cut #3, flange side Figure. 5.21, Error distribution and grid density distribution (izolines greater than 1.0 are shown), (1) - (12) like Figure. 5.20,

Cut #3, flange side Figure. 5.22, Error distribution and grid density distribution (izolines greater than 10.0 are shown), (1) - (12) like Figure. 5.20.

Set #3, cut#5 (Figures 5.23 – 5.25) - summarizing pictures concerning full evaluation of the approximation process and simultaneously experimental data, flange side - horizontal displacements: local error and grid density distribution for different 'error' norms. Detailed description of the pictures is as follows:

Cut #5, flange side, Figure. 5.23, Error distribution and grid density distribution,

- (12) like Figure. 5.20.

In Figures 5.24 and 5.25 area where required grid density is greater than 10.0% is shown for two cuts:

Cut #5, flange side Figure. 5.24, Error distribution and grid density distribution (izolines greater than 1.0 are shown), (1) - (12) like Figure. 5.20,

Cut #5, flange side Figure. 5.25, Error distribution and grid density distribution (izolines greater than 10.0 are shown), (1) - (12) like Figure. 5.20.

As one may see from the presented pictures, the results strongly depend on approximation order and the smoothness parameter value. Namely, if the smoothness parameter is large - data is too smooth, simultaneously this increases the error too (but the errors are not very large, however). If magnitude of the smoothness parameter tends to smaller values, data recovered at experimental points is closer to experimental one, but the data obtained at fictitious points is rougher.

Different error norms indicate different zones of the largest errors. Magnitudes of the norms differ essentially. Higher order norms give larger errors and are more sensitive to changes in the experimental values.

As one may observe, the zero order Sobolev norm indicates completely different zone of the largest errors than the first or second order Sobolev norm. From Figures 5.20-5.25 one may see that cutting area is best traced by second Sobolev semi-norm.

An error analysis has been applied to approximation of numerical data coming from FEM analysis as well. Calculation of the influence coefficient matrix (see [10]) needs approximation of numerical data from FEM mesh nodes to residual stress recovery procedure nodes (not presented here).

6. New adaptive procedure of experiment planning

As a practical result of introduced error analysis, new adaptive procedure of experiments planning is possible.

Experimental method should take into account character of the measured function, it cannot be separated from character of measured physical field. Simply speaking, in regions where gradients of measured field are larger, one requires many

more experimental points. Presented approach gives a theoretical foundation for above mentioned crucial condition in experimental mechanics.

One may distinguish two different situations:

1. it is possible to simulate behavior of measured element or part of structure by means of numerical method (FEM, meshless FDM),

2. it is not possible to simulate experiment numerically.

One may note that the experiment may be repeated or not, if yes, sometimes one has the chance to correct location of experimental points. If not, presented approach defines tools for proper data evaluation and filtering .

The following procedure is proposed for the case when numerical simulation of experiment is possible:

1. Solve problem numerically, with conditions for proper simulation of measured part of a structure or an element as good as possible.

2. Evaluate a'posteriori error and repeat calculation with new mesh (grid) density, to statisfy equidistribution error requirements.

3. Define experimental grid and transfer (project) numerical solution (by means of MWLS approximation) to this grid. Try to recover original solution from experimental grid using experimental grid as a primary grid and numerical grid as a secondary grid. Evaluate a'posteriori error and new experimental grid density function which takes into account equidistribution of an error.

4. If is it possible, change experimental point locations, repeat experiment and evaluate a'posteriori error distribution (now real error).

5. Evaluate measured data using estimated error (or new required experimental grid density) as a reliability index to decide which data have to be removed or taken with lowered weight.

If meshless method is used in above mentioned procedure, numerical simulation of the experiment is very easy, because one may directly use experimental grid as numerical one, without any transformations and additional (approximation) errors.

In the case when numerical simulation of experiment is not possible, procedure is as follows:

1. After experiment evaluate a'posteriori error and calculate new mesh (grid) density of experimental points with equidistribution of error.

2. If is it possible change experimental point locations, repeat experiment and evaluate a'posteriori error distribution.

3. Evaluate measured data using determined error (or new required experimental grid density) as a reliability index to decide which data have to be removed or considered with lowered weight.

7. Final Remarks

Present work is devoted to description and evaluation of the fundamental methods of the physical data approximation and the *a posteriori* error estimation *i.e*. the methods based on differences between original, experimental data (or numerical ones coming from FEM/FDM analysis) and data approximated on fictitious mesh (see [8]).

The *a posteriori* error analysis described above has been applied to the wheel saw cut data and numerical data coming from FEM analysis, using the Meshless Finite Difference approximation. The presented error analysis approach is of great value in determination of the required concentration of experimental points in the zones where the largest stress gradients have occurred.

The current research done on error estimation includes:

– generalization of the Zienkiewicz - Zhu postprocessing estimator concept [17] for elastic problems in solid mechanics and its use in analysis of wheel saw cut data,

– determination of the optimal strategies for refinement of the experimental (or numerical) clouds of points, using different error norms (Sobolev norms up to second order),

– development of postprocessing techniques to enhance the solution accuracy using different number of nodes in stars, different approximation order (*i.e.* 2nd or 3rd order) and additional iterative process to smoothen the largest discrepancies between data on original (experimental) and fictitious (numerical) grids,

– formulation of the new *adaptive approach to experiment planning and carrying out*, taking into account a'posteriori error estimation and distribution of experimental points with equidistributed error,

– analysis of wheel saw cut data, especially for wheel #2 (see R.Czarnek [3]), 5 cuts of the wheel, both flange and 2nd sides of the wheel analyzed,

– analysis of numerical data, coming from FEM analysis, for wheel #2 [11].

Advantages of the error analysis performed on the experimental as well as numerical data (see FEM/FDM analysis [11]) have been shown. A significant step towards a new adaptive analysis (approximation) of the physical data was done. Besides, approach presented here, yields formulation of new requirements against measurements devices possible, thus making way for adaptive experimental data collection.

The proposed further research includes: development of reliable error estimates for computed "physical fields" with the efficiency index close to 1 (approximated fields are very close to original ones), further development of the optimal strategies for 'h' adaptive refinement of the experimental data points cloud, development of adaptive modeling in which certain features of physical models are incorporated and stress analysis of deformation fields in rails and wheels.

8. References

1. Belytschko T., Krongaus Y., Organ D., Flemming M., Krysl P., "Meshless Methods: An Overwiew and Recent Development", *Comp. Meth. in Appl. Mech and Engng*, 139, 3-44, 1996.

2. Bugeda G., Onate E, "New Adaptive Techniques for Structural Problems", *Numerical Methods in Engng'92*, Ch.Chirsh et al. (Editors), Elsevier Science Publishers B.V., 1992.

3. Czarnek R., Experimental Determination of Release Fields in Cut Railroad Car Wheels, DOT/FRA/ORD-96/DOT-VNTSC-FRA-96, Final Report, Cambridge, USA, October, 1996.

4. Demkowicz L., Oden J.T., Rachowicz W., Westerman T.A, "Toward a Universal h-p Adaptive Finite Element Strategy. Part2: A Posteriori Error Estimation", *Computer Methods in Applied Mechanics and Engineering*, 77(1-2)113-180, 1989.

5. Karmowski W., Orkisz J., "Physicall Based Enhanced Analysis of Stresses Using Experimental Data", in: *Quality and Maintenance for Modern Railway Operation*, editor J.J.Kalker et al., pp. 287-296, Delft, 24-26 June, 1992.

6. Karmowski W., Orkisz J., "Physically Based Method of Enhanced of Experimental Data – Concept, Formulation and Application to Identification of Residual Stresses", *Proc. of the IUTAM Symposium on Inverse Problems in Engng Mechanics*, May 11-15 Tokyo, Japan, Springer-Verlag, 61-70, 1993.

7. Krok J., Orkisz J., "Application of the Generalized FDM to Calculation of Arbitrary Loaded Axisymmetrical Massive Structures", *Proc of 28-th Conf. KILiW PAN and KN PZITB*, Krynica, Poland, 1982, 81-90 (in polish).

8. Krok J., New Approach of Error Control in Approximation and Smoothing of Physical Data, Application to wheel Saw Cut Measurements Data, Report to the VNTSC, Cambridge, USA, 1998.

9. Krok J., Orkisz J., "Application of the Generalized FD Approach to Stress Evaluation in the FE Solution", *Int. Conf. on Comp. Mech.*, Tokyo 1986, XII, pp.31-36.

10. Krok J., Orkisz J., "A Unified Approach to the FE Generalized Variational FD Method in Nonlinear Mechanics, Concept and Numerical Approach", in: *Discretization Method in Structural Mechanics, IUTAM/IACM Symposium Vienna 1989*, p. 353-362, Springer-Verlag, 1990.

11. Krok J., Orkisz J., Skrzat A., "Reconstruction of Hoop Stresses in 3D Bodies of Revolution Based on Simulated Saw Cut Data", *XIII Conf. on Comp. Meth. in Mechanics*, Poznań, Poland, 669-676, 1997.

12. Krok J., Orkisz J., "Unified Approach to the Adaptive FEM and Meshless FDM. Concept and Tests", *2nd European Conference on Computational Mechanics*, June 26-29, Cracow, Poland , 2001, p. 1-33.

13. Liszka T., Orkisz J., *The finite difference method at arbitrary irregular grids and its applications in applied mechanics*, Computers and Structers, 11, 83-95, 1980.

14. Liszka T., “An interpolation method for an irregular net of nodes”, *International Journal for Numerical Methods in Engineering*, 20, 1599-1612, 1984.

15. Orkisz J., “The Finite Difference Method”, Part III, in: *Numerical Methods in Mechanics*, in: Springer-Verlag, 1998.

16. Zhu J.Z., Hinton E., Zienkiewicz O.C., “Mesh Enrichment Against Mesh Regeneration Using Quadrilateral Elements”, *Comm. in Num. Meth. in Engng*, Vol. 9, 547-554, 1993.

17. Zienkiewicz O.C., Zhu J.Z., “A Simple Error Estimator and Adaptive Procedure for Practical Engineering Analysis”, *Int. Journ. Num. Meth. Eng.*, 24, 337-357, 1987.

18. Zienkiewicz O.C., Zhu J.Z., “The Superconvergent Patch Recovery and A’Posteriori Error Estimates”, Part 2: Error Estimates and Adaptivity, *Int. J Num Meth Engng*, Vol 33, p. 1365-1382, 1992.

19. Zienkiewicz O.C., Taylor R.L., *Finite Element Method*, Butterworth, Oxford, 2000.

20. Gavette L., Cuesta J.L., Ruiz A., “A Procedure for Approximation of the Error in the EFG Method”, *Int. Journ. Num. Meth. Eng.*, Vol. 53, p. 677-690, 2002.

21. Skrzat A., Orkisz J., Krok J., “Residual Stress Reconstruction in Railroad Car Wheels Based on Experimental Data Measured at Saw Cut Test”, *2nd European Conference on Computational Mechanics*, June 26-29, Cracow, Poland , 2001, p. 1-17.

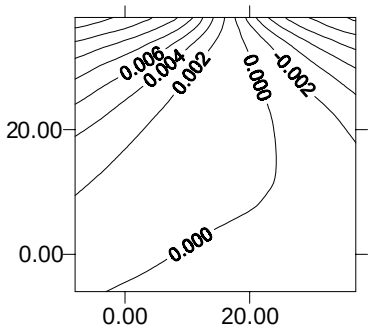

Fig.5.2, Cut #1, Flange side,
horizontal displacements,
original data, min=-1.25E-2, max=1.55E-2

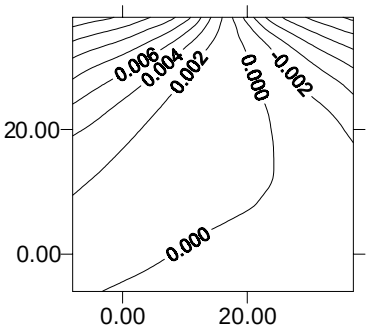

Fig.5.3, Flange side,
horizontal displacements,
approximated data after 7 iterations

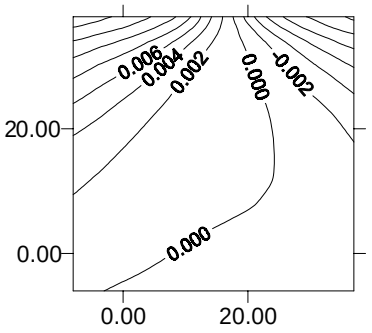

Fig. 5.4, Flange side,
horizontal displacements,
recovery data, no iteration

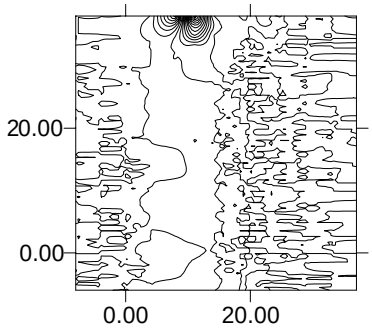

Fig.5.5, Flange side,
Error of the horizontal displacements,
no iterations,
min=1.35E-5, max=7.46E-6, inc=1E-6

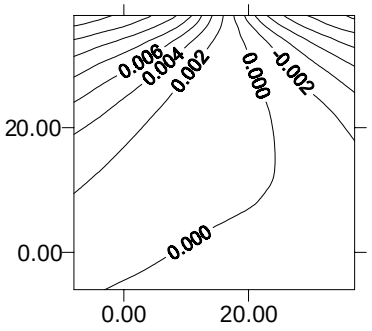

Fig. 5.6, Flange side,
horizontal displacements,
recovery data, after iterations

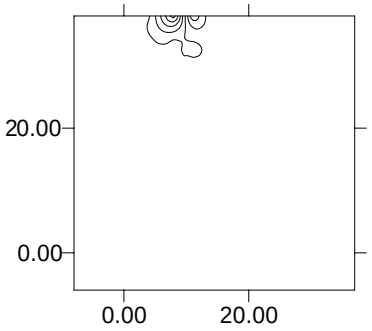

Fig.5.7, Flange side,
error of the horizontal displacements,
after 7 iterations,
min=-1.34E-6, max=2.40E-6, inc=5E-7

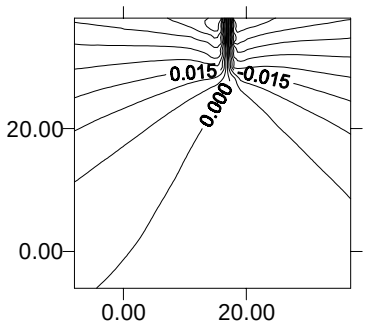

Fig. 5.8, Cut #3, Flange side,
horizontal displacements,
original data, min=-4.48E-2, max=4.33E-2

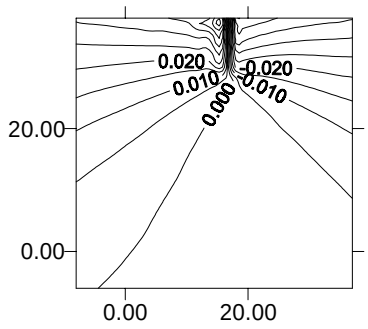

Fig. 5.9, Flange side,
horizontal displacements,
approximated data, after 7 iterations

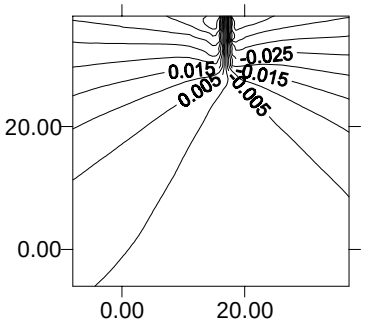

Fig. 5.10, Flange side,
horizontal displacements,
recovery data, no iterations

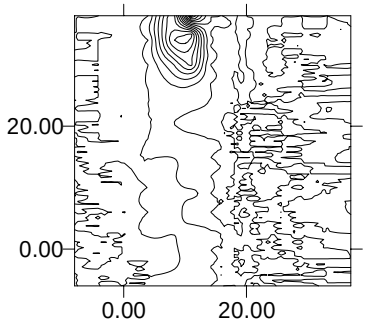

Fig. 5.11, Flange side,
error of the horizontal displacements,
no iteration,
min=-1.47E-4, max=1.10E-4, inc=2E-5

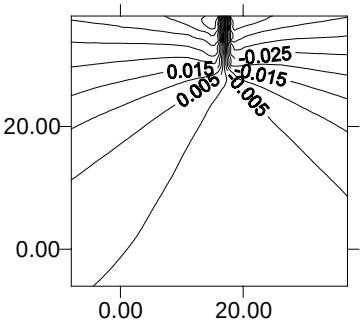

Fig. 5.12, Flange side,
horizontal displacements,
recovery data, after 7 iterations

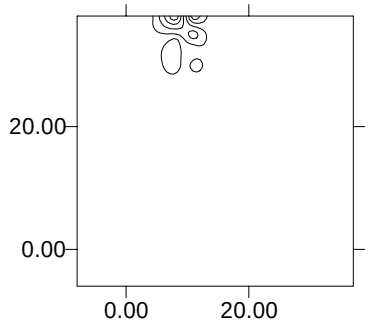

Fig. 5.13, Flange side,
error of the horizontal displacements,
after 7 iterations,
min=-2.12E-5, max=1.35E-5, inc=5E-6

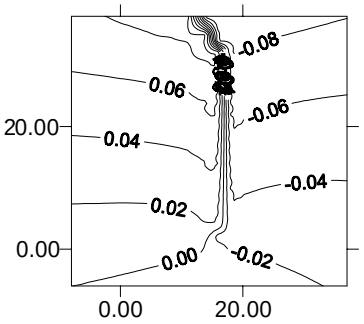

Fig. 5.14, Cut #5, Flange side,
horizontal displacements,
original data, min=-9.49E-2, max=9.00E-2

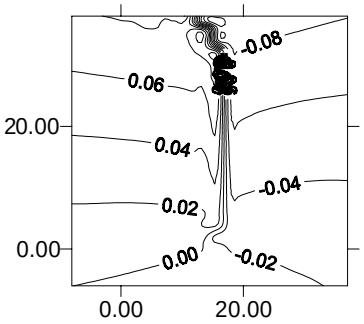

Fig. 5.15, Flange side,
horizontal displacements,
approximated data, after 7 iterations

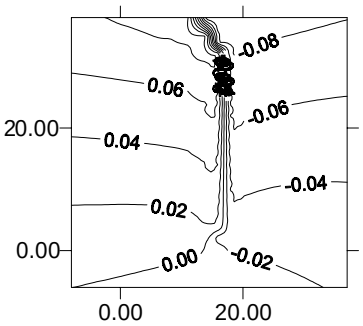

Fig. 5.16, Flange side,
horizontal displacements,
recovery data, no iterations

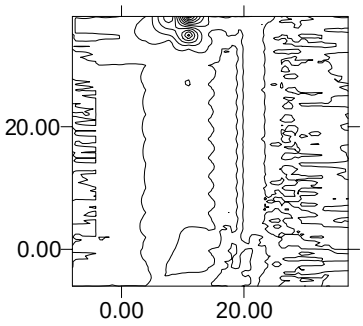

Fig. 5.17, Flange side,
error of the horizontal displacements,
no iteration,
min=-3.25E-3, max=2.72E-3, inc=1E-3

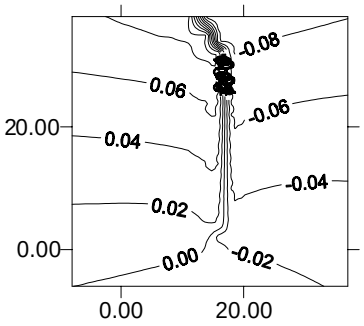

Fig. 5.18, Flange side,
horizontal displacements,
recovery data, after 7 iterations

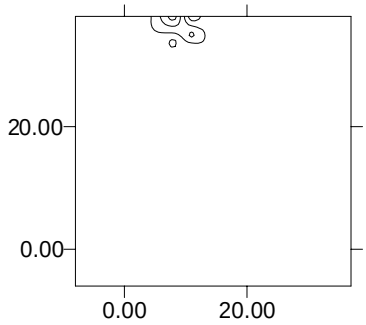

Fig. 5.19, Flange side,
error of the horizontal displacements,
after 7 iterations,
min=-3.41E-4, max=5.54E-4, inc=2E-4

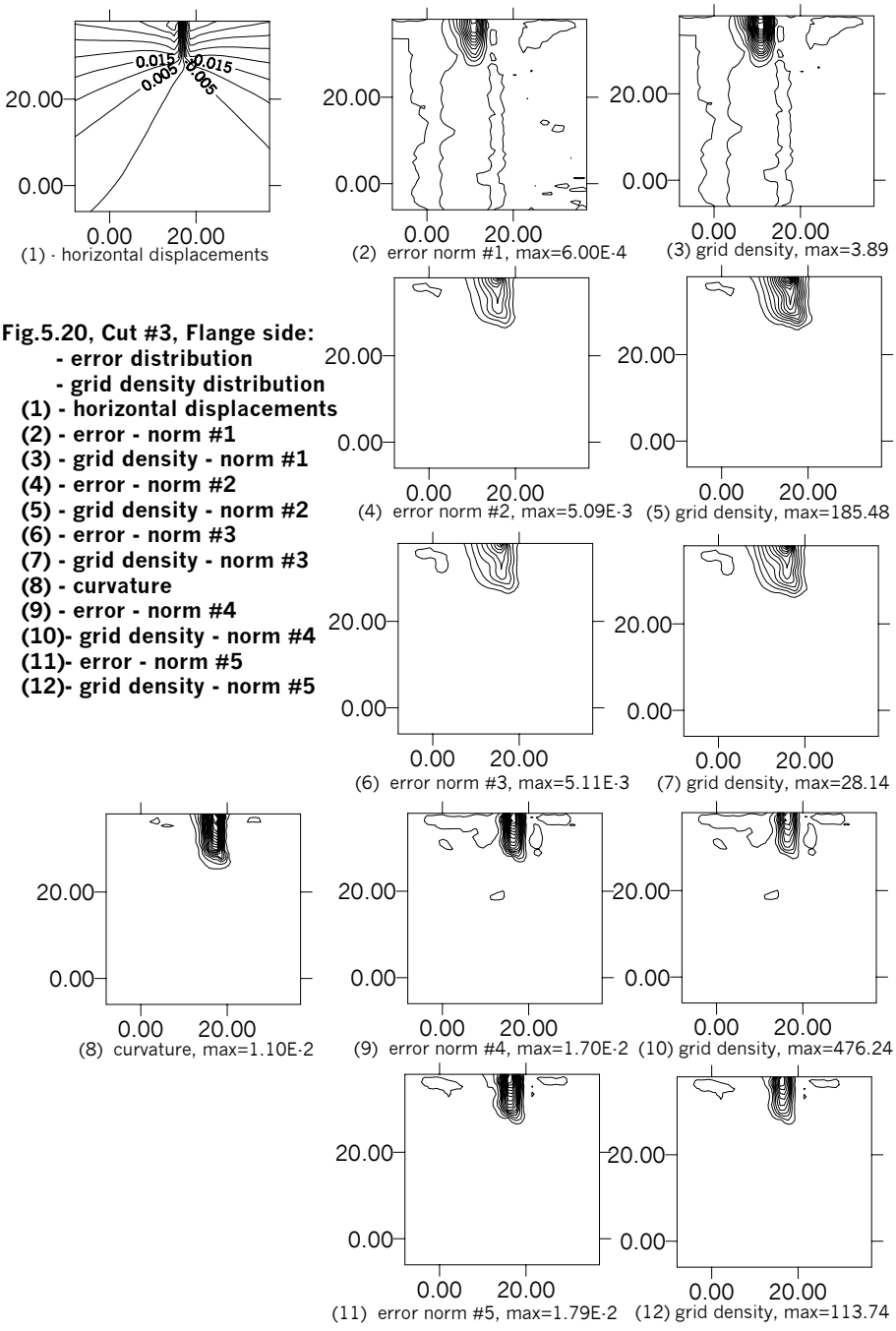

Fig.5.20, Cut #3, Flange side:
- error distribution
- grid density distribution
(1) - horizontal displacements
(2) - error - norm #1
(3) - grid density - norm #1
(4) - error - norm #2
(5) - grid density - norm #2
(6) - error - norm #3
(7) - grid density - norm #3
(8) - curvature
(9) - error - norm #4
(10)- grid density - norm #4
(11)- error - norm #5
(12)- grid density - norm #5

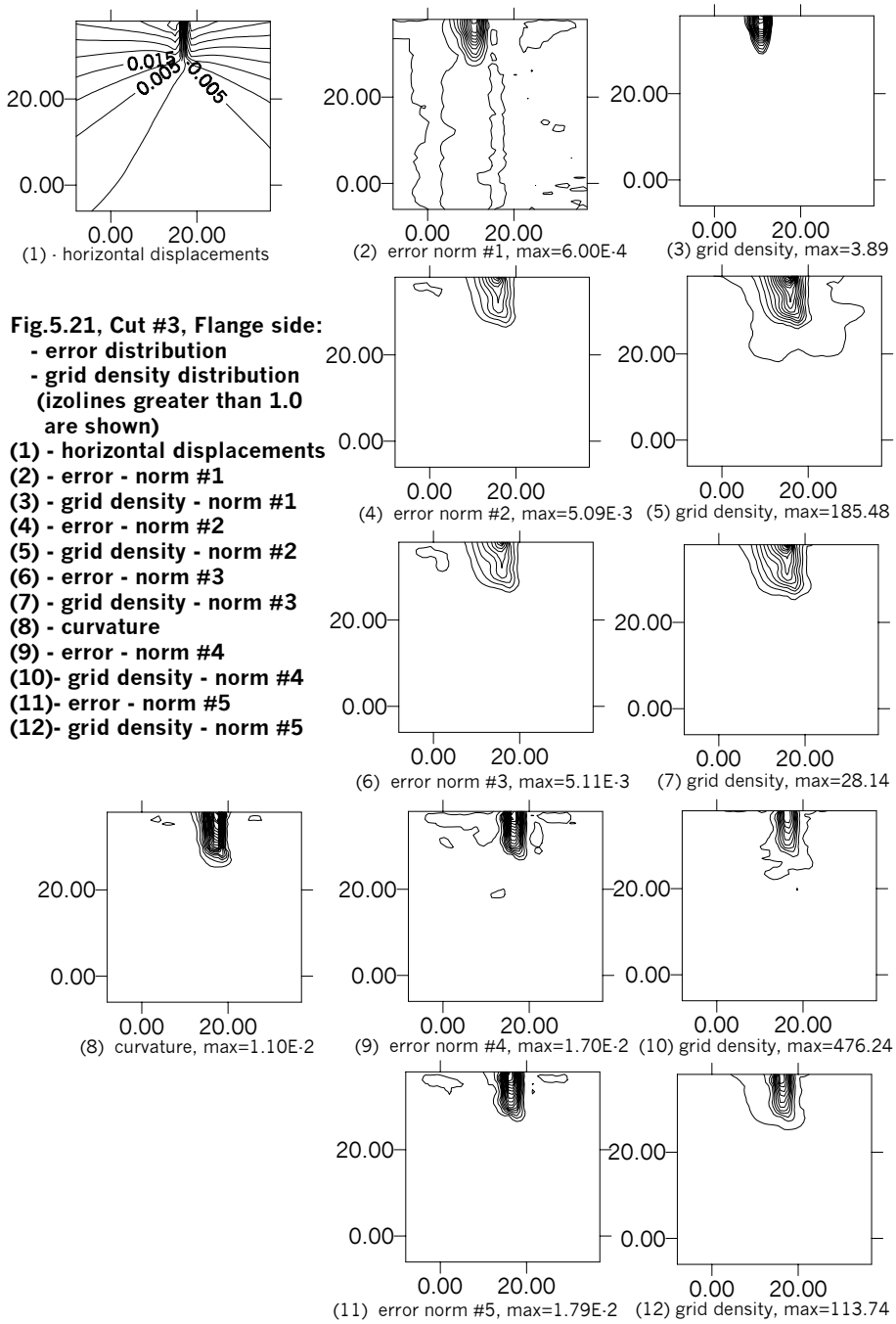

Fig.5.21, Cut #3, Flange side:
- error distribution
- grid density distribution
(izolines greater than 1.0 are shown)
(1) - horizontal displacements
(2) - error - norm #1
(3) - grid density - norm #1
(4) - error - norm #2
(5) - grid density - norm #2
(6) - error - norm #3
(7) - grid density - norm #3
(8) - curvature
(9) - error - norm #4
(10)- grid density - norm #4
(11)- error - norm #5
(12)- grid density - norm #5

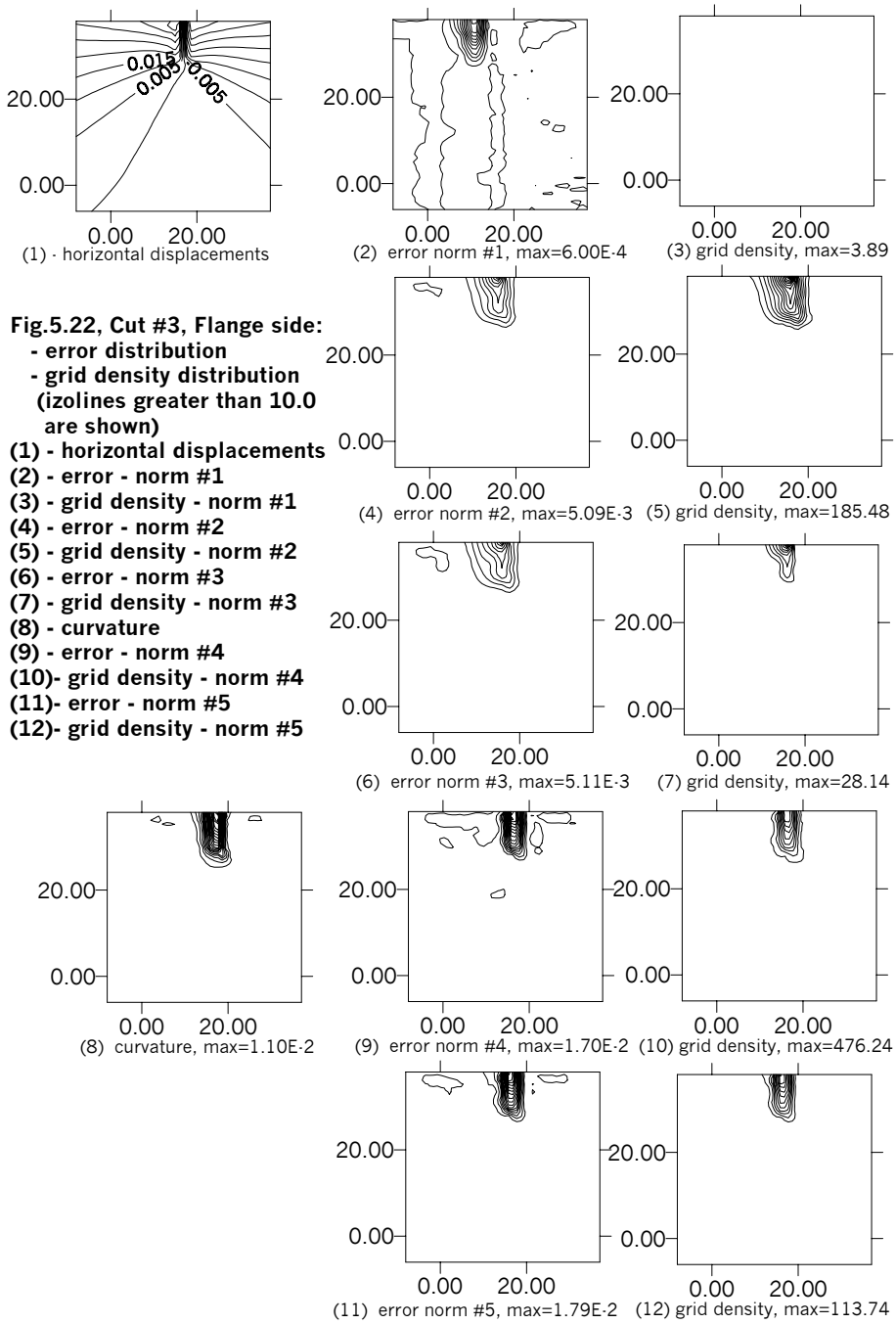

Fig.5.22, Cut #3, Flange side:
- error distribution
- grid density distribution
(izolines greater than 10.0 are shown)
(1) - horizontal displacements
(2) - error - norm #1
(3) - grid density - norm #1
(4) - error - norm #2
(5) - grid density - norm #2
(6) - error - norm #3
(7) - grid density - norm #3
(8) - curvature
(9) - error - norm #4
(10)- grid density - norm #4
(11)- error - norm #5
(12)- grid density - norm #5

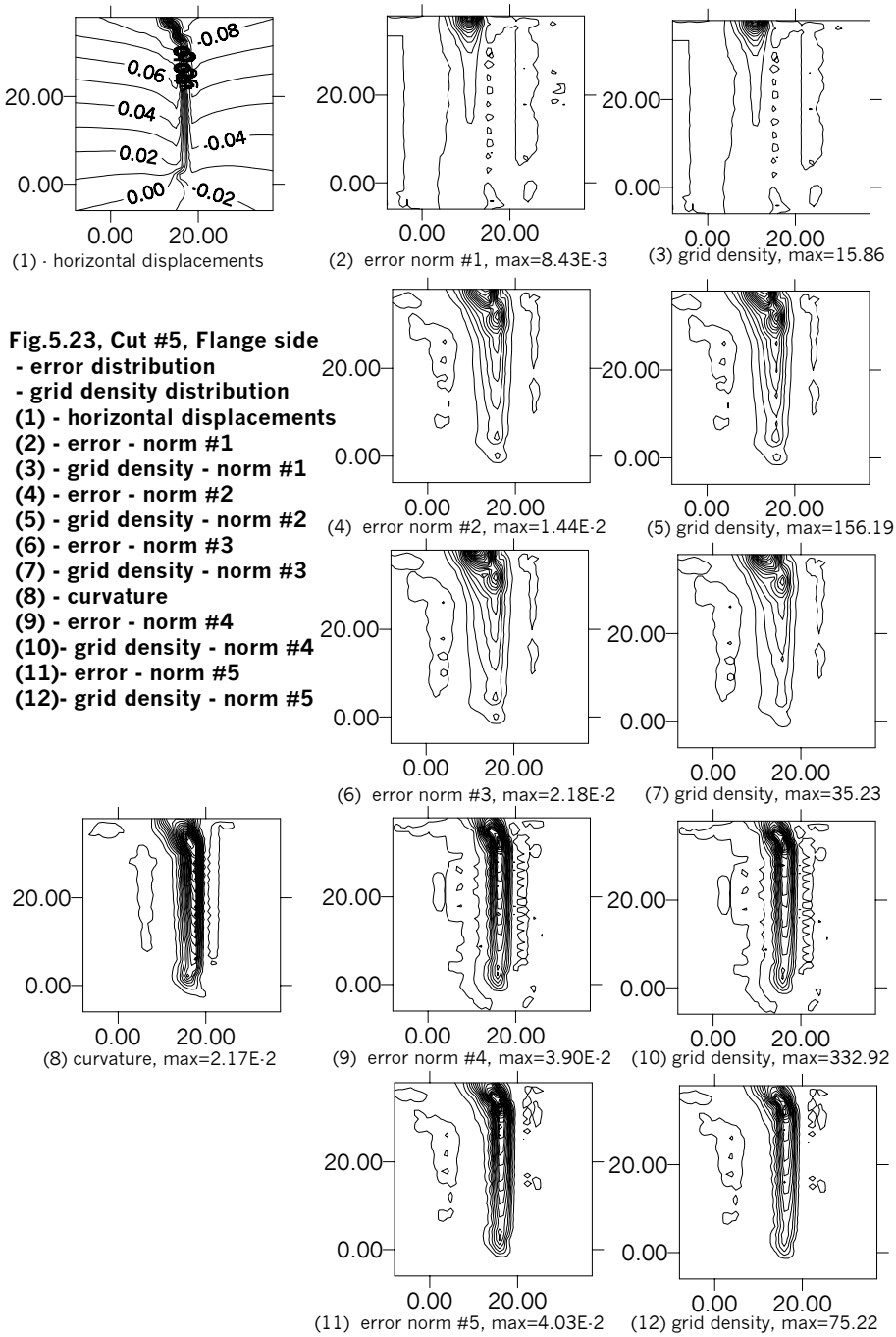

Fig.5.23, Cut #5, Flange side
- error distribution
- grid density distribution
(1) - horizontal displacements
(2) - error - norm #1
(3) - grid density - norm #1
(4) - error - norm #2
(5) - grid density - norm #2
(6) - error - norm #3
(7) - grid density - norm #3
(8) - curvature
(9) - error - norm #4
(10)- grid density - norm #4
(11)- error - norm #5
(12)- grid density - norm #5

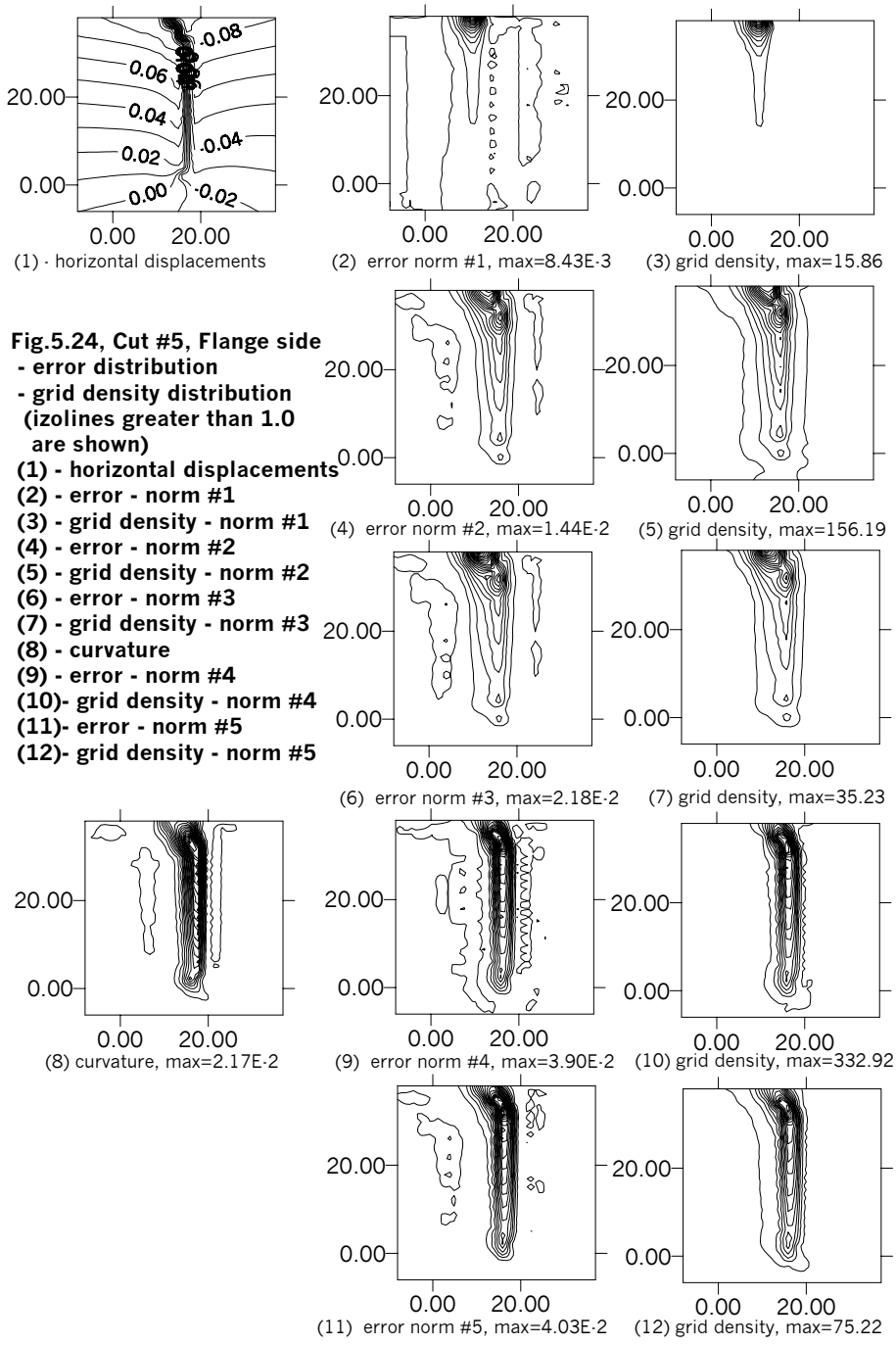

Fig.5.24, Cut #5, Flange side
- error distribution
- grid density distribution
(izolines greater than 1.0 are shown)
(1) - horizontal displacements
(2) - error - norm #1
(3) - grid density - norm #1
(4) - error - norm #2
(5) - grid density - norm #2
(6) - error - norm #3
(7) - grid density - norm #3
(8) - curvature
(9) - error - norm #4
(10)- grid density - norm #4
(11)- error - norm #5
(12)- grid density - norm #5

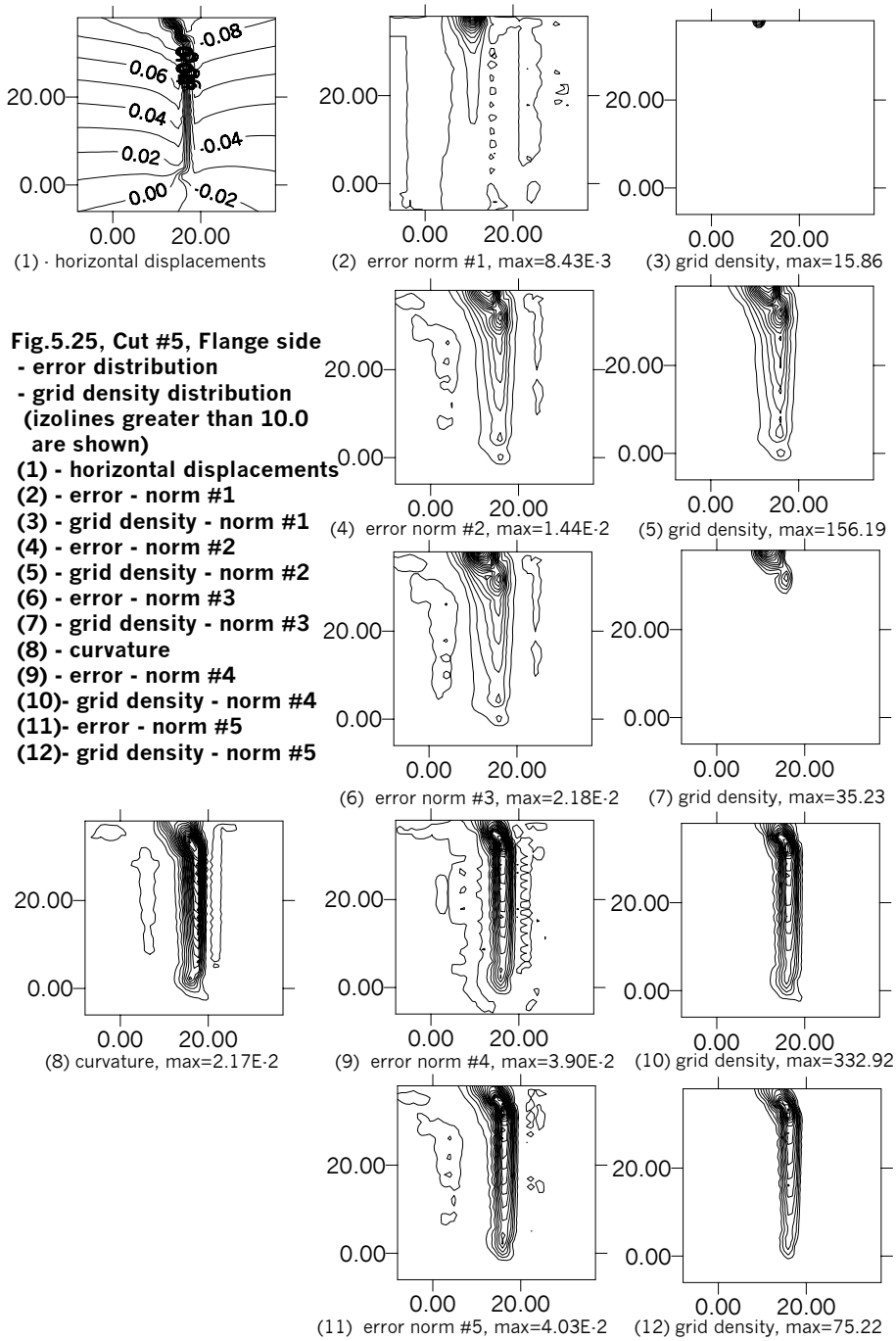

Fig.5.25, Cut #5, Flange side
- error distribution
- grid density distribution
(izolines greater than 10.0 are shown)
(1) - horizontal displacements
(2) - error - norm #1
(3) - grid density - norm #1
(4) - error - norm #2
(5) - grid density - norm #2
(6) - error - norm #3
(7) - grid density - norm #3
(8) - curvature
(9) - error - norm #4
(10)- grid density - norm #4
(11)- error - norm #5
(12)- grid density - norm #5